MEMS Pressure Sensor Array for Aeroacoustic Analysis of the Turbulent Boundary Layer

J. Krause*, R. White*, M. Moeller**, J. Gallman** and R. De Jong***

*Tufts University
200 College Ave, Medford, MA — r.white@tufts.edu
**Spirit AeroSystems, Wichita, KS
***Calvin College, Grand Rapids, MI

ABSTRACT

The design, fabrication, and characterization of a surface micromachined, front-vented, 64 channel (8×8), capacitively sensed pressure sensor array for aeroacoustic testing of the turbulent boundary layer (TBL) is discussed. The array was fabricated using the MEMSCAP polyMUMPs® process, a three layer polysilicon surface micromachining process. An acoustic lumped element circuit model was used to model the system. The results of our computations for the design, including mechanical components, environmental loading, fluid damping, and other acoustic elements are detailed. Theory predicts single element sensitivity of 0.6 mV/Pa at the bandpass output (6 μV/Pa at the preamp output) in the 400-40,000 Hz band. The size of the vent holes has a major impact on low frequency modeled acoustic sensitivity. Laser Doppler Velocimetry shows low frequency electrostatic stiffness and a primary resonant frequency that agree well with the models. Experimental verification of acoustic sensitivity is ongoing.

Keywords: aeroMEMS, microphone array, turbulent boundary layer, polyMUMPs

1 INTRODUCTION

Turbulence has been plaguing transport aircraft designers for over fifty years. A clear and concise definition of turbulence has yet to be made, but Tennekes and Lumley pose seven qualities that characterize turbulence. They present turbulence as being irregular, diffuse, and often associated with large Reynolds numbers. It is a three-dimensional vortical fluctuation following a continuum model and dissipates over time [1]. Several models have been analytically and experimentally obtained to understand the complex nature of turbulence, but as a result of the stochastic nature, a theoretical model is more difficult to obtain. Therefore, using hot wire anemometry, shear stress sensors, and pressure sensors at the microscopic level will help to obtain empirical results describing the phenomena associated with turbulence and more importantly the TBL.

The sources of structural excitation and radiative noise in passenger aircrafts are noise due to the interior environment, the engine, and the fluctuations in wall pressure beneath the TBL. The noise generated by the TBL is considered the most dominant noise source on transport aircrafts [2]. In order to model the structural response of an aircraft, spectral levels at both low and high wavenumbers are needed [3]. The low wavenumber assessment is vital due to the fact that structural resonances take place at low wavenumbers and acoustic noise is generally emitted at low wavenumbers compared to convective turbulent energy [4]. Although low wavenumbers are important for the analysis of acoustic noise generation and structural vibrations, the high convective wavenumbers are where the greatest energy levels are present in the turbulent field, and hence need to be understood. A lack of empirical knowledge as a result of the limits due to conventional instrumentation is one reason for our poor understanding of turbulence [5]. MEMS pressure sensors may alleviate this issue due to their small size and the ability to fabricate multiple microphones in an array. The challenge in MEMS arrays is achieving good matching between elements in the array and across arrays. In addition, due to their small size, the microphones necessarily have low sensitivity.

MEMS pressure sensors have been explored by many researchers over the past 25 years and many review articles can be found on them [6, 7, 8]. Most pressure sensors are developed for auditory applications, biomedical ultrasound arrays, and underwater applications [7]. Few microphones have been developed for aeroacoustic applications, possibly due to the difficulty of surviving the harsh environment. The Interdisciplinary Microsystems Group at the University of Florida Gainesville has done a great deal of work in this area and Martin *et al.* demonstrate a good summary of the previous microphones for aeroacoustic measurement [9].

2 FABRICATION

The fabrication process of the 64 channel capacitive microphone array utilizing the MEMSCAP PolyMUMPs® process along with facilities at Tufts University and Massachusetts Institute of Technology is described. The polyMUMPs process is a foundry process that creates polysilicon structures via surface micromachining with a minimum feature size of 2 μm. The process consists of seven physical layers, including 3 structural, 2 sacrificial and one metal layer. For more information on the PolyMUMPs process, see [10]. *Figure* 1 shows two cross-sections of a single element in the microphone array. The structural diaphragm (top electrode) is made of phosphorus doped polysilicon with a 600 μm diameter and thickness of 3.5 μm. The bottom electrode is 580 μm in diameter, 0.5 μm thick phosphorus doped polysilicon layer that serves as a bottom electrode. The air gap between the diaphragm and the bottom electrode is 2 μm. To prevent stiction during fabrication and while in operation, the bottom of the diaphragm contains 201 dimples, spaced on a 30 μm pitch, with a depth of 1.0 μm. There is also a small corrugation close to the edges of the diaphragm to help relax any tensile residual stresses due to fabrication or deflection.

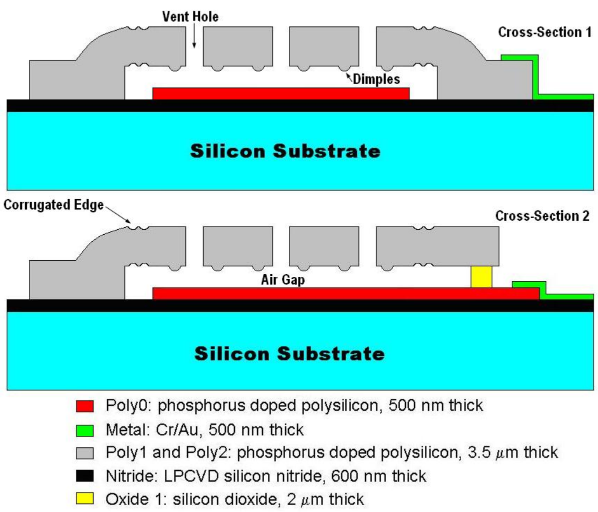

Figure 1: Two cross sections of a single microphone.

There are vent holes through the diaphragm that serve two purposes: (1) introduction of HF etchant to remove the oxide sacrificial layer to create the 2 μm high air gap and (2) act as vent holes to front vent the microphone and allow operation with changing atmospheric pressure. There are 28 holes in the diaphragm with a center-to-center spacing of 100 μm. The vent holes are created using two etches. One etch is a 6 μm diameter hole, while the other is a 4 μm diameter hole. The holes are designed to be concentric and should result in a 4 μm diameter hole through the diaphragm. As manufactured, alignment tolerances result in non-concentric holes, creating irregular shaped holes with a larger area than desired (see *Figure* 2 for an SEM image of this).

The elements are arrayed on a 1 cm $\times$ 1 cm chip in an 8$\times$8 pattern. There are 76 bond pads along the edges of the chip for electrical connection. The direction of flow is top to bottom so the flow does not pass across the bond pads. The element center-to-center pitch in the direction of flow is 1.2625 mm (which allows for multiple 8$\times$8 array to be placed end-to-end to determine low wavenumber information through the larger spatial scale), while the pitch across the flow is 1.1125 mm. Packaging uses a pin grid array package to which the MEMS array is wirebonded. Laser cut spacers allow for the MEMS chip to be mounted flush with the package surface.

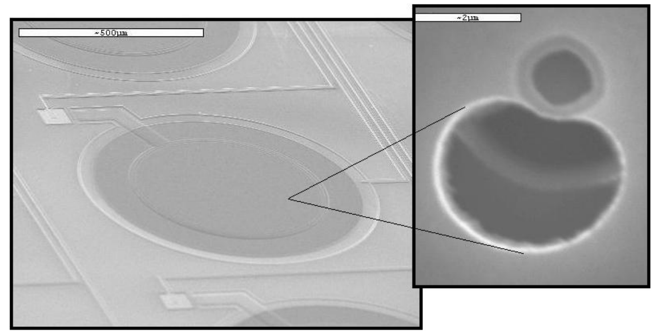

Figure 2: SEM image tilted at a sixty degree angle of an element illustrating the corrugation, wire scheme, vent hole and tunnel concept for static equilibrium of pressure. Diaphragm is 600 μm and vent hole is $\approx$4 μm.

3 MODELING AND DESIGN

A model for one individual microphone in the array is described. For each element in our design, a MATLAB® script was compiled to examine the response electrostatically as well as to a unit pressure. The parameters of the script were computed following an acoustic lumped element circuit diagram shown in *Figure* 3. The compliance, resistance and mass of the microphone were accounted for in the circuit diagram and then implemented into the MATLAB script. The compliances, resistances and mass loading of the microphones were computed using parameters from [9, 11, 12]. Using Beranek's solutions for environmental loading of the air we compute:

$$R_{A1} = \frac{0.1404\rho c}{a^2} \tag{1}$$

$$R_{A2} = \frac{\rho c}{\pi a^2} \tag{2}$$

$$M_{A1} = \frac{8\rho}{3\pi^2 a} \tag{3}$$

$$C_{A1} = \frac{5.94 a^3}{\rho c^2} \tag{4}$$

$$C_{cav} = \frac{V_{gap}}{\rho c^2} \tag{5}$$

where ρ is the density of air, c is the speed of sound, a is the effective radius of the diaphragm (equal to 80% of the actual radius for a circular bending plate), and V_{gap} is the volume of the gap between the diaphragm

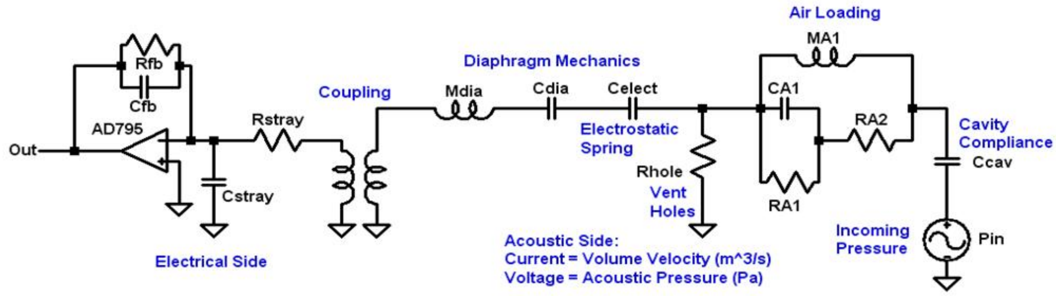

Figure 3: Coupled mechanical-electrical lumped element model.

and bottom electrode. From Martin *et al.* we compute resistance due to the holes in the diaphragm, the compliance of the diaphragm (for a clamped circular bending plate), and the effective mass of the diaphragm (for the first mode of the clamped circular bending plate):

$$R_{through} = \frac{72\mu t_{dia}}{n\pi a_{hole}^4} \tag{6}$$

$$C_{dia} = \frac{\pi a^6(1-\nu^2)}{16Et^3} \tag{7}$$

$$M_{dia} = \frac{9\rho t_{dia}}{5\pi a^2} \tag{8}$$

where μ is the viscosity of air, t_{dia} is the thickness of the diaphragm, n is the number of holes in the diaphragm, a_{hole} is the radius of the holes in the diaphragm, ν is Poisson's ratio, and E is the elastic modulus of the diaphragm. Using Škvor's formula, (S), and calculating a correction factor, (C_f) we can determine the resistance due to the squeeze film damping $(R_{squeeze})$ [9, 13].

$$S = \frac{\pi a_{hole}^2}{C^2} \tag{9}$$

$$C_f = \frac{S}{2} - \frac{S^2}{8 - \frac{1}{4}ln(S) - \frac{3}{8}} \tag{10}$$

$$R_{squeeze} = \frac{12\mu C_f}{n\pi t_{gap}^3} \tag{11}$$

The hole resistance in the circuit model is the series combination of the squeeze film damping, $R_{squeeze}$ and the through-hole damping, $R_{through}$,

$$R_{hole} = R_{squeeze} + R_{through} \tag{12}$$

where C is the center-to-center spacing of holes in the diaphragm. Using the above model for the microphone and using a coupling parameter, N, to relate the pressure to a voltage:

$$N = \frac{V_{bias}\epsilon}{t_{gap}^2} \tag{13}$$

where V_{bias} is the bias voltage applied to the bottom electrode, ϵ is the permittivity of free space, and t_{gap} is the height of the air gap. This coupling parameter gives the acoustic pressure applied to the diaphragm for a given AC voltage on the electrical side, and, equivalently, the current into the electrical side in response to a given volume velocity of the diaphragm.

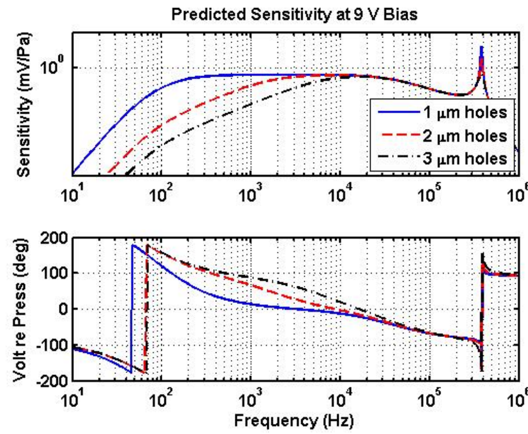

Figure 4: Predicted acoustic sensitivity for a single element with 9 V_{bias}, showing the importance of the vent hole size.

$$P_{electrostatic} = N \cdot V_{ac} \tag{14}$$

$$I = N \cdot U_{dia} \tag{15}$$

The sensitivity (voltage out per Pascal) can be computed as a function of frequency by incorporating the electronics which give the response curve its shape. The model for the receive electronics is a series combination of two single pole passive high pass filters with break frequencies of 60 Hz and 80 Hz, a charge amp with a gain of 100 mV/pC, and a voltage gain stage of 100 with a single pole low pass filter at 40 kHz. The final predicted pressure sensitivity results are shown in *Figure* 4. This is sensitivity at the bandpass output (40 dB above the preamp output in the passband). Varying the size of the vent holes has a major impact on the low frequency response.

4 RESULTS

Laser Doppler velocimetry (LDV) is used to measure the centerpoint vibration of the diaphragm in response to an applied AC voltage plus DC bias. The

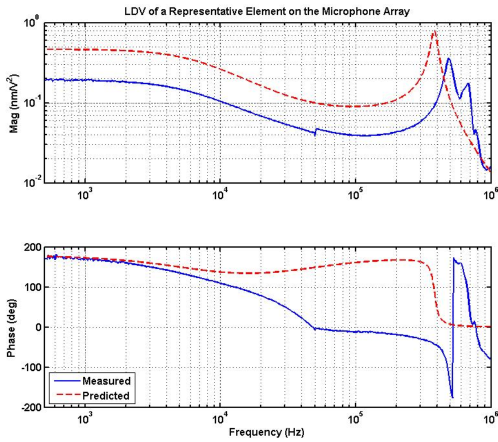

Figure 5: Laser Doppler velocimetry (LDV) measurements as a result of an electrostatic excitation to the microphone.

results of the measurement show a strong, high Q resonance at 480 kHz. The frequency of the resonance is strongly influenced not only by the bending stiffness of the diaphragm, but also by the acoustic stiffness coming from the backing cavity and the environmental acoustic impedance. *Figure* 5 shows a comparison between the measured electrostatic frequency response and the model predictions. The model does a good job of predicting the primary resonance frequency and the shape of the low frequency magnitude curve.

Preliminary tests using prototype electronics (2 channels) in a Faraday cage show acoustic sensitivity that changes with applied bias, as expected. The sensitivity at the bandpass output with 9 V_{bias} is on the order of 1 mV/Pa, similar to the model predictions, but additional testing is required to confirm this.

5 CONCLUSION

A front-vented surface micromachined capacitively sensed microphone for aeroacoustic analysis of the TBL has been fabricated. The microphone utilized the MEMSCAP PolyMUMPs® process as well as facilities at Tufts University's Micro and Nano Fabrication Facility and Massachusetts Institute of Technology's Microsystems Technology Laboratory. Device modeling agrees well with electrostatic testing using laser Doppler velocimetry. Preliminary acoustic testing shows microphone sensitivity, but frequency response measurements of acoustic sensitivity have not yet been obtained. Controlling the geometry of the vent holes is crucial to the low frequency response of the microphones. The high frequency resonance at 480 kHz is strongly influenced by the acoustic compliances coming from the vented air gap and external environmental loading. The next step in the array development is plane wave tube calibration against a reference microphone and array modeling. Packaging for wind tunnel testing is also underway.

References

[1] H Tennekes and J. L. Lumley. *A First Course in Turbulence*. The MIT Press, 1972.

[2] J. F. Wilby and F. L. Gloyna. Vibration measurements of an airplane fuselage structure II. jet noise excitation. *Journal of Sound and Vibration*, 23(4):467–486, August 1972.

[3] W. R. Graham. A comparison of models for the wavenumber-frequency spectrum of turbulent boundary layer pressures. *Journal of Sound and Vibration*, 206(4):541–565, October 1997.

[4] W.L. Abraham and B.M. Keith. Direct measurements of turbulent boundary layer wall pressure wavenumber-frequency spectra. *Journal of Fluids Engineering*, 120:29–39, March 1998.

[5] G. M. Corcos. Resolution of pressure in turbulence. *The Journal of the Acoustical Society of America*, 35(2):192–199, February 1962.

[6] G. M. Sessler. Acoustic sensors. *Sensors and Actuators A: Physical*, 26(1-3):323–330, March 1991.

[7] P. R. Scheeper, A. G. H. van der Donk, W. Olthuis, and P. Bergveld. A review of silicon microphones. *Sensors and Actuators A: Physical*, 44(1):1–11, July 1994.

[8] Lennart Löfdahl and Mohamed Gad-el-Hak. Mems applications in turbulence and flow control. *Progress in Aerospace Sciences*, 35:101–203, 1999.

[9] David T. Martin, Jian Liu, Karthik Kadirvel, Robert M. Fox, Mark Sheplak, and Toshikazu Nishida. A micromachined dual-backplate capacitive microphone for aeroacoustic measurements. *Journal of Microelectromechanical Systems*, 16(6):1289–1302, 2007.

[10] Jim Carter, Allen Cowen, Busbee Hardy, Ramaswamy Mahadevan, Mark Stonefield, and Steve Wilcenski. Polymumps design handbook: a mumps®process. Internet, 2005.

[11] Leo L. Beranek. *Acoustics*. Acoustical Society of America, 1996.

[12] Lawrence E. Kinsler, Austin R. Frey, Alan B. Coppens, and James V. Sanders. *Fundamentals of Acoustics: Fourth Edition*. John Wiley & Sons, 2000.

[13] D. Homentcovschi and R.N. Miles. Viscous damping of perforated planar micromechanical structures. *Sensors and Actuators A: Physical*, 119(2):544–552, April 2005.